Influence of steering effects on strain detection in AlGaInN/GaN heterostructures by ion channelling

A Redondo-Cubero , K Lorenz , N Franco , S Fernández-Garrido , R Gago , P J M Smulders , E Muñoz , E Calleja[1] and E Alves

ISOM and DIE, ETSI Telecomunicación, Universidad Politécnica de Madrid, E-28040 Madrid, Spain
Centro de Micro-Análisis de Materiales, Universidad Autónoma de Madrid, E-28049 Madrid, Spain
Instituto Tecnológico e Nuclear, Estrada nacional 10, 2686-953 Sacavém, Portugal
Instituto de Ciencia de Materiales de Madrid, Consejo Superior de Investigaciones Científicas, E-28049 Madrid, Spain
Nuclear Solid State Physics, Materials Science Centre, Groningen University, Nijenborgh 4, 9747 AG Groningen, The Netherlands

Abstract

Ion steering effects in the interface of heterostructures can strongly influence the shape and position of angular channelling scans leading to considerable error in the determination of strain by ion channelling. As an example, this paper presents channelling measurements on a near-lattice-matched AlGaInN/GaN heterostructure which show no shift between the angular scans from the quaternary layer and the underlying GaN substrate although high resolution x-ray diffraction data confirm the presence of strain in the layer. Such 'anomalous' behaviour was studied by means of Monte Carlo simulations for nitride ternary and quaternary films in the whole composition range. The simulations show that the thickness, magnitude of the distortion of the strained lattice and energy of the probing beam are critical parameters controlling the impact of steering. Three composition/strain regions were established for a typical beam of 2 MeV alpha particles corresponding to different intensities of the steering potential and in which strain measurements by ion channelling are (a) correct, (b) possible but require corrections and (c) not possible due to steering effects.

(Some figures in this article are in colour only in the electronic version)

1. Introduction

Elastic strain is a fundamental issue in semiconductor materials, affecting not only crystal quality but also electronic properties such as effective mass, bandgap and carrier density [1]. The strain indeed plays an important role in the development of high-power electronic and optoelectronic devices based on III-nitride compounds due to the large values of the piezoelectric coefficients [2–4]. These materials have attracted great interest in the last decade due to the possibilities of bandgap engineering and the heterostructure technology they can support [5]. The conventional growth of GaN is normally performed on sapphire substrates where, due to the lattice mismatch to GaN of ~16%, the crystal quality is considerably affected by the presence of dislocations and strain [6]. Therefore, there is a considerable interest in strain-free heterostructures with low dislocation densities, which seems feasible by the increasing availability of free standing GaN substrates. The AlGaInN quaternary system provides independent control over the band gap and the in-plane lattice parameter with respect to ternary nitrides, allowing the design of strain-free devices with a wide range of operating wavelengths. Furthermore, the electronic parameters of these GaN-based devices are easily controlled by elemental composition and thickness.

The most frequent method for determining the strain state of crystalline thin films is x-ray diffraction (XRD) [7]. However, this technique does not provide in-depth information and, in some cases, the interpretation of the scan is difficult due to the overlapping of reflection peaks. This inconvenience in fact takes place for AlGaInN and AlInN layers grown close to the lattice match conditions to GaN [8]. In addition, the compositional analysis of ternaries carried out by XRD is highly dependent on the exact knowledge of the lattice parameters and elastic constants of binary nitrides. Furthermore, in the particular case of quaternary nitrides compositional analysis by XRD is not possible due to the lack of sufficient fitting parameters. Therefore, the importance of using complementary techniques for the determination of composition, strain and crystal quality in these situations is clear.

Ion channelling is another approach for assessing structural properties in crystalline materials [9, 10]. The underlying physics of channelling processes is based on the directional effects that take place when a charged particle beam is aligned with a major symmetry direction of the crystal and penetrates deep into the lattice with significantly reduced yield of backscattered projectiles [11]. In this way, channelling-based techniques have a high sensitivity to any lattice perturbation such as extended defects (dislocations, stacking faults, etc), strain, impurities or implantation damage [12]. Rutherford backscattering spectrometry in combination with channelling (RBS/C) provides structural and compositional information with depth resolution [13], yielding complementary information to XRD.

Above a critical angle of incidence between the probing beam and channel axis the particles are not able to remain channelled and the backscattering yield increases [11]. This strong angular dependence of scattering yield in the experimental angular scans is characterized by a typically symmetric dip, which reaches a minimum for perfect alignment of the beam with the lattice channel. Width and minimum yield of the dip are the fundamental parameters for the analysis, mainly related to the critical angle, the vibration amplitude of the atoms and lattice defects. The strain state of semiconductor heterostructures is often calculated directly from the angular shift between the channelling dips of the layer and the substrate, since the minimum yield should appear at different angles for strained films in a scan performed within a plane that contains both axes (of the film and the substrate). This angular shift corresponds to the kink angle, $\Delta\theta$, the angle between the same low index crystal direction in the film and the substrate. In this way, the potential of these RBS/C analyses for strain determination has been successfully shown on several semiconductor systems [14–16], and hence it can be considered as one of the best alternatives to solve the restrictions in the XRD analysis. Even so, recent RBS/C measurements of strain in different heterojunctions (based on GaAs [17], GaN [18], InP [19], and Si [20]) have shown substantial limitations. Actually, it has been proven that, when the kink angle is lower than the critical angle, RBS/C does not reproduce the real strain values because of the presence of steering effects. Due to these effects, it has been shown that the experimental angular scans across the axial direction can present 'anomalous channelling' effects with asymmetric dips to double minimum configurations [17,18].

The manifestation of these phenomena is generally explained in Lindhard's analytical theory as a consequence of the statistical equilibrium of the ion flux distribution in the channel [21]. Monte Carlo (MC) methods have shown, however, that this hypothesis is not always verified, depending on the thickness and the role of focusing effects [22, 23]. Therefore, MC simulations represent a very helpful approach to understand and correct the steering effects additionally taking into account several parameters of the ion–solid interaction such as thermal vibrations of atoms and dechannelling of particles in the different layers [24–26]. When they are incorporated in the analysis, errors in the direct strain calculation can be eliminated [18].

In this paper, we report a comparative study for the determination of strain on AlGaInN/GaN heterostructures using RBS/C and XRD. XRD shows the presence of strain but angular scans from RBS/C experiments carried out across the $(\bar{2}\,1\,1\,3)$ axis did not present the expected shift, asymmetries or double minimum structure. The lack of sensitivity to strain of RBS/C can be ascribed to steering effects as confirmed by MC simulations. Moreover, MC simulations also showed that steering effects can be considerably important even for relatively high values of strain when the layers are thick enough to reach the equilibrium flux distribution.

2. Experiment

A strained AlGaInN/GaN heterostructure was grown by rf plasma-assisted molecular beam epitaxy (PA-MBE) on a $(0\,0\,0\,1)$ GaN template (3.6 μm thick) on sapphire. A 100 nm thick GaN buffer layer was grown at 730 °C under Ga-rich conditions to obtain a smooth and flat surface. Next, a 250 nm thick layer of AlGaInN was then grown at 600 °C under metal-rich conditions. More details about growth conditions can be found elsewhere [27, 28].

High resolution XRD reciprocal space maps (RSMs) of the AlGaInN/GaN bilayer were acquired in a high resolution D8Discover diffractometer from Bruker-AXS with an asymmetric 2-bounce Ge$(2\,2\,0)$ monochromator and a scintillation detector using monochromatic Cu ($K_{\alpha 1}$) radiation.

RBS/C experiments were performed with a 2 MeV $^4He^+$ beam, spot of 1 mm^2. Backscattered ions were detected by silicon surface barrier detectors (energy resolution of 16 keV) placed at 165° and 170.1° in the IBM geometry. A 3-axis goniometer was employed to control the crystal position for angular scans with an accuracy of 0.01°. Angular scans across the $\langle 0\,0\,0\,1\rangle$ and $\langle\bar{2}\,1\,1\,3\rangle$ axes were used to determine the crystal quality and the strain state of the film, respectively. Random spectra for compositional analysis were acquired by rotating the sample during the measurement. Both aligned and random spectra were simulated by the RBX code [29].

3. MC simulations

MC simulations were carried out using the code FLUX [30]. A total number of 10 000 ions was used to guarantee low

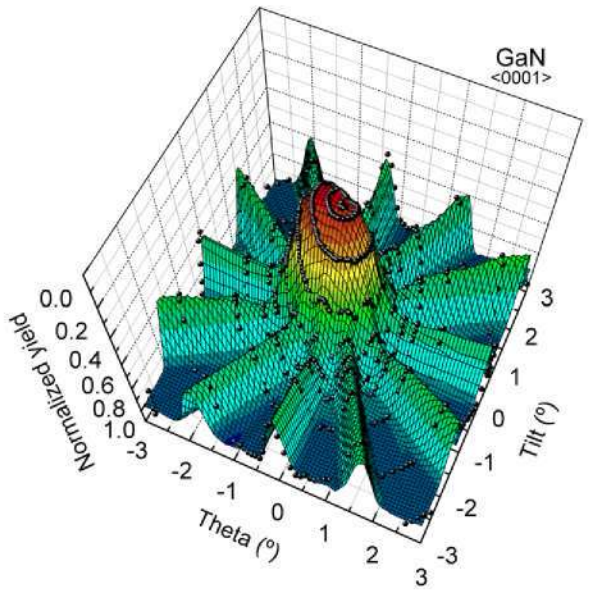

Figure 1. Angle-resolved scan across the ⟨0 0 0 1⟩ axis of wurtzite type GaN. Solid spheres represent experimental points. The yield axis scale is inverted for a better view of the central dip.

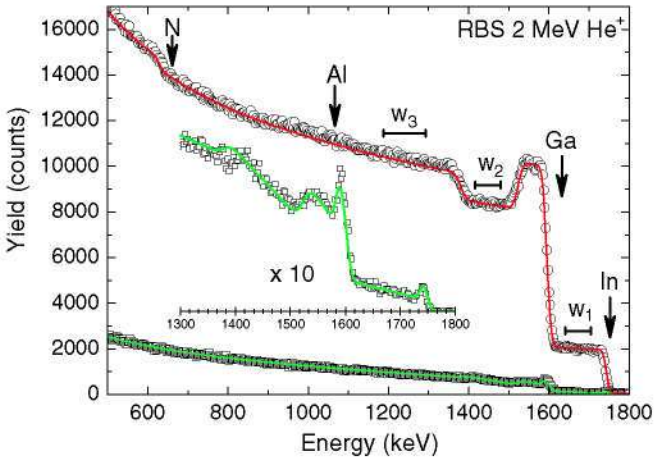

Figure 2. Random and ⟨0 0 0 1⟩ aligned spectra (circles and squares) from RBS/C experiments performed with 2 MeV He^+ ions. Composition and dechannelling of the layer were fitted by the simulation (solid line). The inset shows details of the aligned spectrum. The three selected energy windows for experimental scans and MC simulations are also exposed.

statistical error. The universal Ziegler–Biersack-Littmark potential was assumed for the calculations of the individual ion–solid collisions [31]. The wurtzite lattice ($P6_3mc$) was selected for the crystal, with the incident beam randomly distributed over the unit cell. The simulated angular scan was performed in the $\langle \bar{2}\,1\,1\,3 \rangle$ axis along the $(1\,0\,\bar{1}\,0)$ plane, being the normalized yield derived from the close encounter probability for different angles. In the simulation, channelling processes were not directly incorporated since they appear as a consequence of the binary collisions of ions with the lattice.

For the simulations a two-layer model was employed: a first layer with the nitride compound of a fixed composition and the second with the GaN substrate. The strain state of the nitride compound was incorporated by means of a rotation matrix between both layers, using the kink angle as an input. This kink angle was calculated for a given film composition by determining the lattice parameters of a relaxed film from Vegard's law and those of a strained layer by combining Vegard's law and elasticity theory (Poisson's equation). The kink angle is then derived by $\Delta\theta = \theta^{\mathrm{GaN}} - \theta^{\mathrm{film}}$ where θ is the angle between the tilted axis and the growth direction. In the present case the angle between the ⟨0 0 0 1⟩ and the $\langle -2\,1\,1\,3 \rangle$ axes is given by $\tan\theta = a/c$. Vibration amplitudes ($u_2 = \sqrt{2}u_1$) of the participant atoms were 0.08 Å (Al), 0.11 Å (Ga), 0.13 Å (In) and 0.09 Å (N). Values for Al and Ga are in good agreement with the current literature [32, 33], although the Debye temperature for GaN is still under debate [34]. The vibrational amplitude for In atoms was fixed with the best fit because of the lack of references.

4. Results and discussion

4.1. RBS/C analysis of the AlGaInN/GaN heterostructure

The GaN template used for the growth of the quaternary nitride was first analysed by means of RBS/C. Figure 1 shows the angular-resolved scan around the ⟨0 0 0 1⟩ crystallographic axis of GaN (note that the z-axis scale is inverted in the graph). Twelve minima are clearly visible in the drawing, revealing the well-known wurtzite structure of GaN [5]. The intensity of the minima can be used to select the crystallographic planes for the analysis of strain, $\{2\,\bar{1}\,\bar{1}\,0\}$ dips being deeper than the $\{1\,0\,\bar{1}\,0\}$ ones [35]. The minimum yield for alignment with the ⟨0 0 0 1⟩ axis was 1.76(6)%, demonstrating the excellent quality of the crystal.

Figure 2 shows random and ⟨0 0 0 1⟩ aligned RBS/C spectra of the AlGaInN/GaN bilayer, together with the simulated spectra (solid lines) extracted from RBX. The fitting of the experimental data was done assuming a single-layer model. Since the Rutherford cross-section is higher for heavy elements, the sensitivity to In and Ga is higher than for the lighter elements. Moreover, the Al and N signals are overlapped with the Ga signal from the GaN buffer layer. Both effects preclude a direct quantification of both elements. Therefore, a stoichiometric nitride (50% of N in the sample) was assumed for the fitting and the Al concentration was derived from the deficiency in In and Ga. The resulting composition for the quaternary nitride was found to be $Al_{0.02}Ga_{0.90}In_{0.08}N$.

The ⟨0 0 0 1⟩ aligned spectrum (lower graph and inset in figure 2) reveals a minimum yield $\chi_{\mathrm{min}} = 4.3(1)\%$ for the In-signal close to the surface, confirming the high crystalline quality of the AlGaInN film. Despite this, a significant increment in the fraction of dechannelled ions (3.6% according to the simulation) with respect to GaN is observed for the quaternary layer. Since the dechannelled ions from the GaN layer are only 0.32%, this fact suggests the presence of intrinsic defects in the quaternary compound.

Figure 3 shows the experimental angular scans around the $\langle \bar{2}\,1\,1\,3 \rangle$ direction, acquired in steps of 0.05°. The integrals for the different energy windows (see figure 2) correspond to the signal from In (w1) and Ga (w2) within the quaternary layer and Ga (w3) from the GaN buffer layer. As shown,

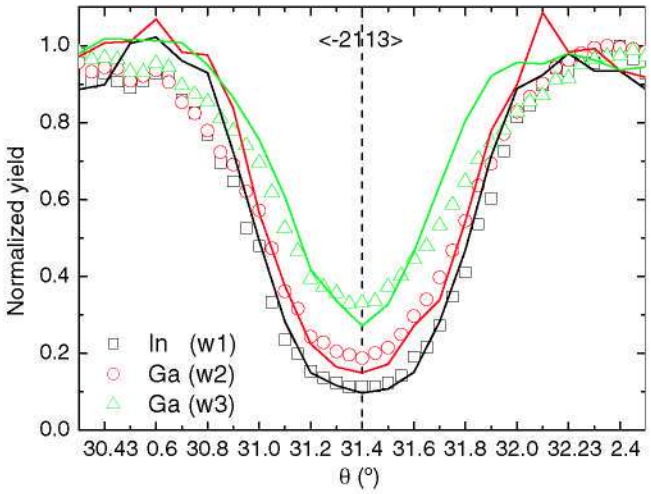

Figure 3. Experimental angular scans across the $\langle\bar{2}\,1\,1\,3\rangle$ axis and MC simulations. Selected energy windows were studied as depicted in figure 2. No shift is visible between the Ga-dip from the substrate and the dips from the film revealing the presence of steering effects.

neither an asymmetry nor a peak shift appears in the scans for the three selected energy windows. *A priori*, this means that the AlGaInN layer is not strained or that our experimental set-up is not sensitive to strain. As shown below, XRD analysis shows that the layer is strained and, therefore, the latter applies.

4.2. XRD analysis of the AlGaInN/GaN heterostructure

The RSMs of the $Al_{0.02}Ga_{0.90}In_{0.08}N$/GaN heterostructure for the $(0\,0\,0\,4)$ and $(1\,0\,\bar{1}\,5)$ planes are shown in figure 4. The fact that the $(0\,0\,0\,4)$ reflection of the film and the buffer are on a horizontal line shows that there are no macroscopic tilts between the crystal planes of both layers. The vertical line crossing the $(1\,0\,\bar{1}\,5)$ GaN reflection represents the positions for pseudomorphic material. The slight deviation of the AlGaInN reflection from this position and its asymmetry shows that the layer is partially relaxed. The slight elongation of the AlGaInN reflection towards the one of GaN points to a compositional grading which is, however, not strong enough to be seen in the RBS spectra. This fact could be related to a first growth stage in which the film starts to grow coherent with slightly lower InN content and then starts to relax and higher InN molar fractions are incorporated into the layer leading to larger c lattice parameters. Such compositional pulling effects are frequently observed in InGaN layers on GaN [36].

The maximum of the $(1\,0\,\bar{1}\,5)$ reflection was found at $(Q_x, Q_z) = (59.91\,\mathrm{nm}^{-1}, 22.77\,\mathrm{nm}^{-1})$, while a totally relaxed material would appear at the position $(Q_x, Q_z) = (60.16\,\mathrm{nm}^{-1}, 22.57\,\mathrm{nm}^{-1})$ as estimated using Vegard's law [37] and marked in figure 4(*b*). The lattice parameters of both layers were extracted from the maps, since Q_x and Q_z are inversely proportional to a and c, respectively. In this way, the a and c values for the GaN and AlGaInN layers, respectively, were found to be $(a, c) = (3.183(2)\text{Å}, 5.190(2)\text{Å})$ and $(a, c) = (3.186(2)\text{Å}, 5.244(2)\text{Å})$. From a relaxed $Al_{0.02}Ga_{0.90}In_{0.08}N$ film (composition derived from

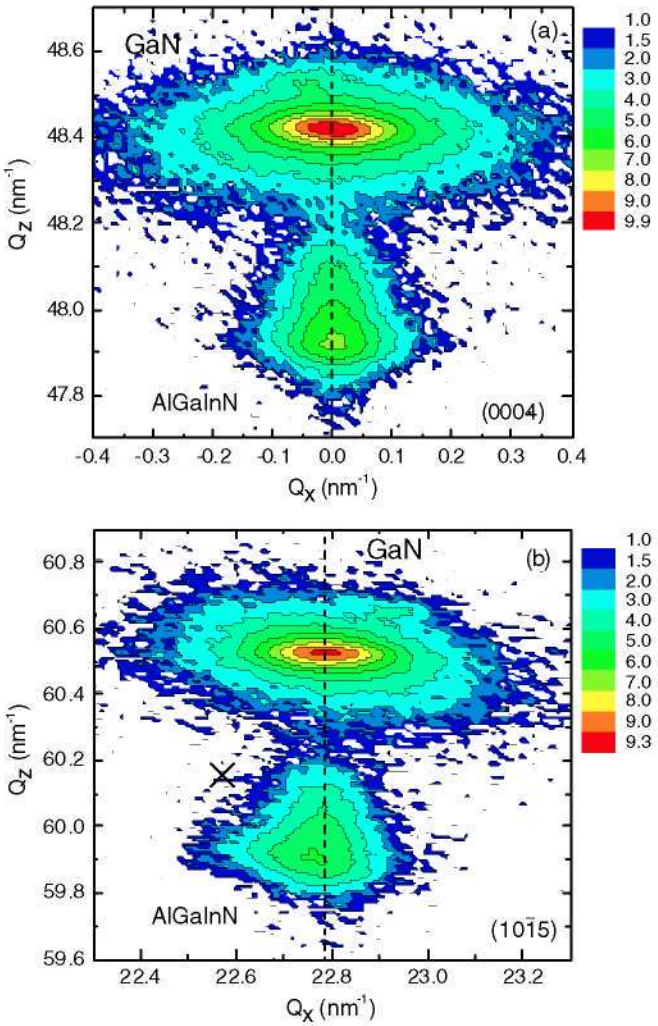

Figure 4. RSMs from HR-XRD measurements around the $(0\,0\,0\,4)$ and $(1\,0\,\bar{1}\,5)$ reciprocal lattice points. The analysis shows that the quaternary film is under compressive strain with a tetragonal distortion of -1.32%. Colour scale represents the intensity (counts) in logarithmic scale. Expected position for a totally relaxed material (by using Vegard's law) is also marked.

RBS), the corresponding lattice parameters of the quaternary layer assuming Vegard's law are $(a_0, c_0) = (3.215\,\text{Å}, 5.244\,\text{Å})$. With these data, parallel and perpendicular strain of the AlGaInN layer were calculated as $\varepsilon^{||} = (a - a_0)/a_0$ and $\varepsilon^{\perp} = (c - c_0)/c_0$. Thus, values of $\varepsilon^{|} = -0.0090(6)$ and $\varepsilon^{\perp} = 0.0042(4)$ were obtained. The resulting tetragonal distortion ($\varepsilon_T = \varepsilon^{||} - \varepsilon^{\perp}$) was -1.32%, indicating that the quaternary layer was grown under compressive strain.

The angle θ between the $\langle 0\,0\,0\,1\rangle$ and the $\langle\bar{2}\,1\,1\,3\rangle$ axes of the film and the GaN buffer layer, being located at $\sim 31.6°$ along the $(1\,0\,\bar{1}\,0)$ plane, can be calculated from $\tan\theta = a/c$. The results from RSMs reveal that a kink angle of $\Delta\theta = -0.24°$ is present between the $\langle\bar{2}\,1\,1\,3\rangle$ axes of the film and the buffer layer, which should become visible in the angular scan across the $\langle\bar{2}\,1\,1\,3\rangle$ axis. However, as seen in figure 2, the expected $\Delta\theta$ is not visible in the angular scan across the $\langle\bar{2}\,1\,1\,3\rangle$ axis. This proves that, for the experimental configuration used, the RBS/C analysis is not sensitive to the strain within the layer.

4.3. MC simulations of RBS/C data using FLUX

4.3.1. Effect of the AlGaInN layer thickness. The anomalous behaviour observed in the RBS/C data (no visible shift between the angular scans corresponding to the $\Delta\theta$ expected for a strained AlGaInN layer) can only be explained if steering effects at the AlGaInN/GaN interface are taken into account. In fact, following Lindhard's formula $\psi_1 = (2Z_1Z_2e^2/Ed)^{1/2}$, the theoretical critical angle along the $\langle\bar{2}\,1\,1\,3\rangle$ axis for Ga atoms is 0.695°, which is ~3 times higher than the calculated $\Delta\theta$. Thus, most ions entering the GaN substrate will be able to modify their trajectory without suffering significant large angle scattering events.

To better understand the steering effects, figure 3 compares MC simulations of the dips along the $\langle\bar{2}\,1\,1\,3\rangle$ axis with the experimental data. In the model, a 250 nm layer of $Al_{0.02}Ga_{0.90}In_{0.08}N$ on GaN substrate was simulated. The measured lattice parameters for GaN and $Al_{0.02}Ga_{0.90}In_{0.08}N$ lead to a kink angle of $\Delta\theta = -0.24°$, which was used as a fixed input parameter. The slight misfit between simulation and experiment can be explained by restrictions in the FLUX code, which does not take into account lattice defects. These defects, however, have been observed in the RBS/C spectra, since the AlGaInN dechannelling rate was 3.6 times higher than that for the GaN substrate.

The insensitivity to $\Delta\theta$ in the angular scans is attributed to steering effects at the interface due to the large thickness of the quaternary layer. Indeed, MC simulations predict that the close encounter probability for the GaN layer is highly dependent on the thickness of the first AlGaInN layer. This situation is related to the mean free path ($\lambda_\perp$) of He^+ ions inside the $\langle\bar{2}\,1\,1\,3\rangle$ channel. This parameter can be calculated from the relation $1/\lambda_\perp = (\pi^2/4)Nda\psi_1^2/\psi$, derived by Lindhard [11]. In our present situation this gives $\lambda_\perp = 55.2$ nm (taking $\psi_1 = \psi$), which is 4.5 times lower than the thickness of the layer. In such conditions He^+ ions can reach the interface without the typical oscillatory behaviour that takes place at the beginning of the process of channelling, enhancing the steering towards the substrate.

The previous assumption is confirmed by further simulations of the angular scans for $\langle\bar{2}\,1\,1\,3\rangle$ in the GaN buffer of structures with the same quaternary composition but for different film thicknesses (from 10 to 250 nm), as shown in figure 5. In the graph, $\theta = 0$ corresponds to the position of the minimum for the surface film. For thin quaternary layers ($< \frac{1}{2}\lambda_\perp$ nm) the change in close encounter probability in the interface (not shown) is dependent on the sign of the incidence angle. In this configuration, RBS/C is sensitive to $\Delta\theta$, as derived by the simulated angular shift (SAS) for the w3 region (in good agreement with the input value of −0.24°). For thicknesses of $\sim\lambda_\perp$ a strong asymmetry is still visible in the dip, indicating that flux oscillations are not completely removed. A double minimum configuration then appears. For thick layers ($>2\lambda_\perp$) the close encounter probability becomes independent of the sign of the incidence angle leading to symmetric channelling dips. This is accompanied by the decay of ion oscillations (normally appearing in the second period [21]) clearly visible when plotting the close encounter probability as a function of depth (not shown). Thus, for large thickness values, the $\Delta\theta$ stays undetectable by RBS/C and no shift is visible in the dip of the SAS, in agreement with the experiments described in section 4.1.

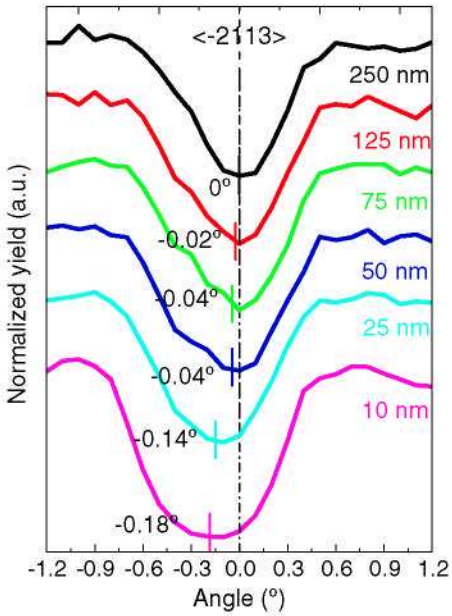

Figure 5. MC simulations of angular scans for an $Al_{0.02}Ga_{0.90}In_{0.08}N$/GaN heterostructure with different thicknesses of the quaternary nitride. The dip corresponds to the Ga signal from the GaN layer (w3). The SAS coincides with the input kink angle for low thicknesses.

4.3.2. Effect of the strain state. Although the thickness of the layer is a critical parameter for the steering of ions, there is a limit for the maximum strain that allows this behaviour. To explore this issue, MC simulations were performed for different values of tetragonal distortion. For simplicity, a pseudomorphic 125 nm thick layer was considered in all cases, since this thickness is higher than $2\lambda_\perp$ but it is less time-consuming in the simulations and corresponds to the thickness of previously studied AlInN layers [18]. Ternary $Al_xGa_{1-x}N$, $In_xGa_{1-x}N$ and $Al_xIn_{1-x}N$ compounds were studied, varying the x parameter to elaborate a complete map. The a parameter of the lattice was fixed as 3.189 Å (relaxed value of GaN) and the expected c lattice parameter for fully strained compounds was calculated taking into account the composition and known values for C_{13} and C_{33} coefficients [38] and following Poisson's equation for elastic deformation, $\varepsilon^\perp = -2(C_{13}/C_{33})\varepsilon^{||}$. Tetragonal distortion was set as an input in the simulation via the kink angle.

For each simulation, the SAS was calculated by a Gaussian fitting of the simulated channelling dip and compared with the value of $\Delta\theta$ used as an input in the simulations, obtaining the relative error (RE). Figure 6 shows the results of RE for the case of a fully strained $Al_xIn_{1-x}N$/GaN bilayer with different $\Delta\theta$ (corresponding to different compositions). Three regions can be clearly distinguished in the graph, depending on the intensity of the steering potential. For values of $|\Delta\theta| > 1.5°$, the steering effects are negligible and the RE is inferior to 5%, meaning that the SAS reproduces the $\Delta\theta$ value. In this region the experimental angular scan can be used directly

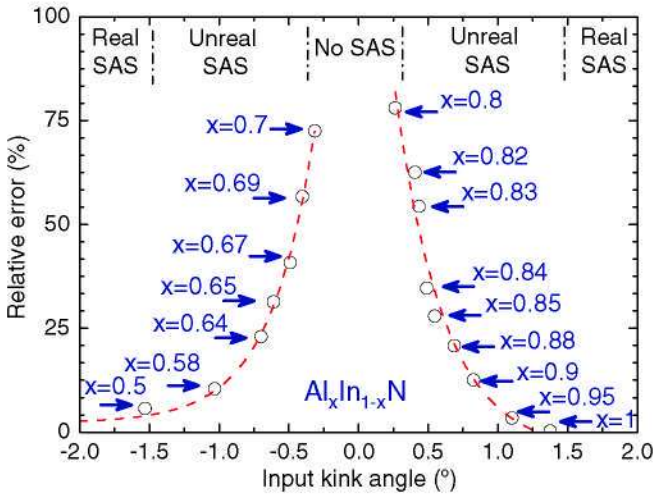

Figure 6. RE of the SAS from MC data (circles) and exponential fit (dashed line) for a 125 nm thick $Al_xIn_{1-x}N$ layer on GaN. Three regions are clearly distinguished, corresponding to different intensities of the steering effects.

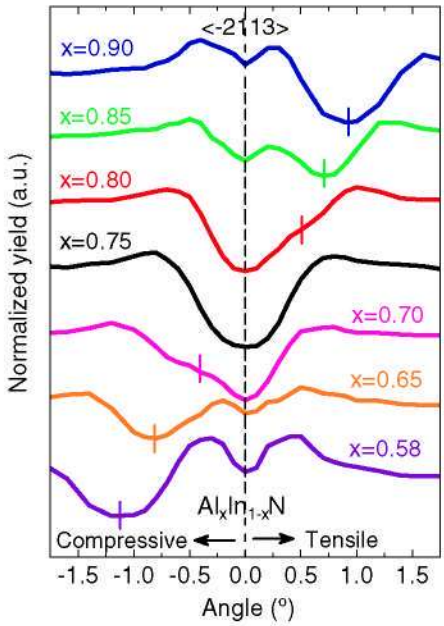

Figure 7. MC simulations of different strained $Al_xIn_{1-x}N$/GaN heterostructures. The modification of the mole fraction (x) results in different strain states, but only some of them can be well resolved due to the steering effects.

to obtain the strain state of the layer. However, for lower values ($1.5° > |\Delta\theta| > 0.5°$) the presence of steering effects becomes more important, and double minimum configurations are visible in the dip of the GaN buffer. In this range, a large fraction of the ions is still able to bend their trajectory at the interface and then SAS does not correspond to $\Delta\theta$. Indeed, RE is higher than 5% and grows with decreasing $\Delta\theta$. This behaviour can be fitted by an exponential function (dashed line in the graph). The correct $\Delta\theta$ can be determined from experimental scans only when MC simulations are used to fit the experimental data [18]. For values of $|\Delta\theta| < 0.5°$, the potential is intense enough to make the shift in the scan undetectable and just a slight asymmetry is observable in the dip. Hence, $\Delta\theta$ cannot be directly measured or fitted by MC calculations.

The transition between these stages is shown in figure 7. With the increasing value of x in the $Al_xIn_{1-x}N$ layer, the in-plane strain state can be modified from compressive to tensile. For $x \sim 0.75$, the SAS is zero because for a completely strained layer with this composition both the a and c lattice parameters are identical with the values of GaN. Furthermore, for compositions close to the real lattice match (the a parameter of relaxed $Al_{0.73}In_{0.17}N$ is the same as for GaN) the strain is very low and the two components of the dip coming from directly and indirectly channelled particles are mixed resulting in asymmetric dips. In those cases a two-Gaussian fitting was used to extract the corresponding SAS, being the first Gaussian centred in the $\theta = 0$ position. When the strain is increasing ($x < 0.7$ and $x > 0.8$) the component associated with $\theta = 0$ (bent ions) disappears progressively, and the RE is rapidly falling.

Figure 8 summarizes the study in the $Al_xGa_{1-x}N$, $In_xGa_{1-x}N$ and $Al_xIn_{1-x}N$ compounds including non-pseudomorphic growth. The molar fraction (x) of these ternary nitrides was varied yielding different $\Delta\theta$ from fully strained to totally relaxed conditions (solid lines in the graph). Points represent the SAS from MC calculations, and the dashed lines correspond to a RE of 5%, 25% and 75%. As can be observed, the presence of steering effects drastically diminishes the capability of detection of the strain state from RBS/C. This situation is particularly important when $\Delta\theta$ is lower than the critical angle ($|\Delta\theta| < 0.5°$), which is the case for low values of strain. The composition of the layer slightly affects the SAS (note that error lines are not constant), but seems to play a minor role in the steering of ions through the interface. Although regions where no SAS is visible are significantly large, MC simulations can still be used to calculate the strain of the layer in several circumstances. It should be noted that steering effects can be reduced for higher beam energies because of the decreased critical angle. Furthermore, steering effects can be suppressed in layers with low crystal quality where strong dechannelling already takes place in the nitride film [8].

5. Conclusions

In this study, RBS/C and XRD experiments on a strained $Al_{0.02}Ga_{0.90}In_{0.08}N$/GaN heterostructure were reported. The compositional and structural analysis obtained from the combination of both techniques shows that the quaternary layer was partially relaxed with a remaining tetragonal distortion of -1.32% in the film. Such a strain state leads to a kink angle between the $\langle\bar{2}\,1\,1\,3\rangle$ axis of the film and that of the GaN buffer layer of $\Delta\theta = -0.24°$. However, experimental angular scans from RBS/C along the $\langle\bar{2}\,1\,1\,3\rangle$ axis revealed no shift between scans of the GaN buffer and the AlGaInN signals. Such anomalous behaviour is explained in terms of the strong steering potential at the interface.

MC simulations of the RBS/C angular scans reveal good agreement with experimental data and support the role of steering effects despite the limitations of the FLUX code (it

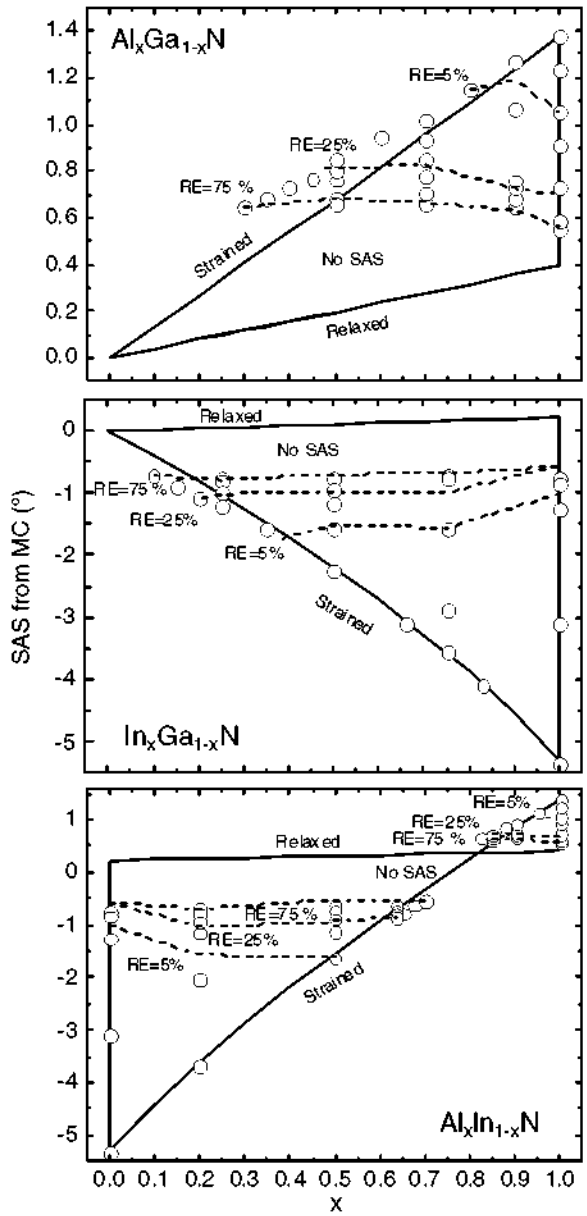

Figure 8. Maps of the regions which can and cannot be assessed by RBS/C (from MC simulations). Solid lines represent theoretical conditions for fully strained and totally relaxed films. Dashed lines correspond to RE of 5%, 25% and 75%. Points show the SAS from MC calculations corresponding to different grades of strain. Increasing RE accompanies the progressive decrease in the input value of the strain state.

does not allow simulating dechannelling due to the presence of defects in the quaternary layer). The relevant role of the quaternary layer thickness on the close encounter probability has been demonstrated. The influence of steering effects on RBS/C strain determination was verified even for high values of strain. It was shown that the RE in the strain state calculation (corresponding to the error that is made if the strain state is determined directly from the shift of experimental angular scans) grows exponentially as the $\Delta\theta$ decreases. Three regions were distinguished corresponding to different intensities of the steering effects: for low $\Delta\theta$ (similar a/c ratios for film and substrate and low strain) it is *not* possible to determine the strain by RBS/C; for intermediate $\Delta\theta$ a correction is required to account for steering effects; and for high $\Delta\theta$ (high lattice mismatch and strain) the strain can be determined directly from the experimental RBS/C scans. The exact boundaries for these regions also depend on the layer thicknesses and the beam energy.

Acknowledgments

This work has been carried out within the KORRIGAN project (EU-FP6 contract no MOU 04/102.052/032). The authors acknowledge financial support by grants PTDC/FIS/66262/2006 (FCT, Portugal), FIS2006-12253-C06-02 (MEC, Spain), CCG07-UAM/MAT-1882 (CAM, Spain) and MOU 04/102.052/032 (EU-FP6).

References

[1] Sun Y, Thompson S E and Nishida T 2007 *J. Appl. Phys.* **101** 104503
[2] Suzuki M and Uenoyama T 1998 *J. Cryst. Growth* **189** 625
[3] Shan W, Hauenstein R J, Fischer A J, Song J J, Perry W G, Bremser M D, Davis R F and Goldenberg B 1996 *Phys. Rev.* B **54** 13460
[4] Bernardini F, Fiorentini V and Vanderbilt D 1997 *Phys. Rev.* B **56** R10024
[5] Morkoç H 1999 *Nitride Semiconductors and Devices* (Berlin: Springer)
[6] Liu L and Edgar J H 2002 *Mater. Sci. Eng.* R **37** 61
[7] Birkholz M 2006 *Thin Film Analysis by X-Ray Scattering* (Weinheim: Wiley-VCH)
[8] Lorenz K, Franco N, Alves E, Pereira S, Watson I M, Martin R W and O'Donnell K P 2008 *J. Cryst. Growth* **310** 4058
[9] Feldman L C, Mayer J W and Picraux S T 1982 *Materials Analysis by Ion Channelling* (New York: Academic)
[10] Gemmell D S 1974 *Rev. Mod. Phys.* **46** 129
[11] Lindhard J 1965 *Mat. Phys. Medd. K. Dan. Vidensk. Selsk.* **34** 14
[12] Tesmer J R and Nastasi M 1995 *Handbook of Modern Ion Beam Material Analysis* (Pittsburg, PA: MRS)
[13] Bird R C and Williams J S 1989 *Ion Beams for Materials Analysis* (London: Academic)
[14] Pereira S, Correia M R, Pereira E, O'Donnell K P, Alves E, Sequeira A D and Franco N 2001 *Appl. Phys. Lett.* **79** 1432
[15] Holländer B, Vescan L, Mesters S and Wickenhäuser S 1997 *Thin Solid Films* **292** 213
[16] Selen L J M 2001 Ion-channeling on nanostructured semiconductors *PhD Thesis* Technische Universiteit Eindhoven
[17] Wu C, Yin S, Zhang J, Xiao G, Liu J and Zhu P 1990 *J. Appl. Phys.* **68** 2100
[18] Lorenz K, Franco N, Alves E, Watson I M, Martin R W and O'Donnell K P 2006 *Phys. Rev. Lett.* **97** 85501
[19] Cohen G M, Ritter D, Richter V and Kalish R 1999 *Appl. Phys. Lett.* **74** 43
[20] Matsushita T, Sakai W, Nakajima K, Suzuki M, Kimura K, Agarwal A, Gossmann H-J, Ameen M and Harimac H 2006 *Nucl. Instrum. Methods.* B **249** 432
[21] Davidson B A, Feldman L C, Bevk J and Mannaerts J P 1987 *Appl. Phys. Lett.* **50** 135
[22] Barrett J H 1973 *Phys. Rev. Lett.* **31** 1542
[23] Fearick R W 2000 *Nucl. Instrum. Methods.* B **164** 88
[24] Robinson M T and Oen U S 1963 *Phys. Rev.* **132** 2385
[25] Barrett J H 1971 *Phys. Rev.* B **3** 1527

[26] Seppälä A 2001 Ion beam channeling studies of compound semiconductor materials *PhD Thesis* Report Series in Physics, Helsinki
[27] Fernández-Garrido S, Redondo-Cubero A, Gago R, Bertram F, Christen J, Luna E, Trampert A, Pereiro J, Muñoz E and Calleja E 2008 *J. Appl. Phys.* **104** 83510
[28] Fernández-Garrido S, Pereiro J, González-Posada F, Muñoz E, Calleja E, Redondo-Cubero A and Gago R 2008 *J. Appl. Phys.* **103** 46104
[29] Kótai E 1994 *Nucl. Instrum. Methods.* B **85** 588
[30] Smulders P J M and Boerma D O 1987 *Nucl. Instrum. Methods.* B **29** 471
[31] Ziegler J F, Biersack J P and Littmark U 1985 *The Stopping and Range of Ions in Solids* (Oxford: Pergamon)
[32] Gabe E, Le Page Y and Mair S L 1981 *Phys. Rev.* B **24** 5634
[33] Yoshiasa A, Koto K, Maeda H and Ishii T 1997 *Japan. J. Appl. Phys.* **36** 781
[34] Roder C, Einfeldt S, Figge S and Hommel D 2005 *Phys. Rev.* B **72** 85218
[35] Holländer B, Mantl S, Mayer M, Kirchner C, Pelzmann A, Kamp M, Christiansen S, Albrecht M, Strunk H P 1998 *Nucl. Instrum. Methods.* B **136** 1248
[36] Pereira S, Correia M R, Pereira E, O'Donnell K P, Trager-Cowan C, Sweeney F and Alves E 2001 *Phys. Rev.* B **64** 205311
[37] Vegard L 1921 *Z. Phys.* **5** 17
[38] Wright A F 1997 *J. Appl. Phys.* **82** 2833